Animal Behaviour 136 (2018) 159–172

Contents lists available at ScienceDirect

Animal Behaviour

journal homepage: www.elsevier.com/locate/anbehav

Volume-concentrated searching by an aerial insectivore, the common swift, *Apus apus*

Emmanuel de Margerie [a,*], Cécile Pichot [a], Simon Benhamou [b]

[a] CNRS, Université de Rennes 1, Université de Caen Normandie, Laboratoire d'éthologie animale et humaine, Rennes, France
[b] CNRS, Centre d'Ecologie Fonctionnelle et Evolutive, Montpellier, France

ARTICLE INFO

Article history:
Received 31 August 2017
Initial acceptance 13 October 2017
Final acceptance 6 November 2017
Available online 6 February 2018
MS. number: 17-00702R

Keywords:
3D optical tracking
aerial predation
aero-ecology
flight behaviour
foraging behaviour
movement ecology

How predators search for prey is a cornerstone question in behavioural ecology, which has yet to be investigated for animals foraging in 3D airspace. Do insectivorous birds such as swifts (Apodidae), swallows and martins (Hirundinidae) use similar strategies to those performed by terrestrial predators in 2D, or do they rely on different spatial search strategies because of some properties of the aerial open space? We addressed this question in the common swift, one of the most aerial birds, using a novel 3D optical tracking method. The analysis of fine-scale flight tracks revealed how birds distribute their presence in 3D space while foraging near their breeding colony. Common swifts concentrated the time spent per volume unit by adopting a tortuous path, and, to a much lesser extent, by decreasing their movement speed. By independently observing the birds' posture on tracking images, we were able to identify the occurrence of putative prey captures along flight tracks. We show that swifts' presence was concentrated mainly in the vicinity of prey captures, unveiling a volume-concentrated search (VCS) strategy in this aerial insectivore. This is an extension in 3D of the area-concentrated search classically described in terrestrial 2D space. VCS can (but does not necessarily) take place in thermal updrafts, where small insects can be concentrated in patches. In contrast to terrestrial and aquatic predators that can easily slow down or stop their movement in profitable places, a different speed–cost relationship underlying aerial movement prevents swifts from stopping in prey patches and explains why these birds rely mainly on movement tortuosity to perform intensive search. Our study thus shows how some physical properties of the environment can modulate the way an animal concentrates its search in profitable places.

Since the airspace has been recognized as a habitat for flying animals (Diehl, 2013), aero-ecology receives growing interest, supported by the advent of radar techniques for scanning the aerosphere for birds, bats and insects (e.g. Frick et al., 2012; Chapman et al., 2015; Horton, Doren, Stepanian, Farnsworth, & Kelly, 2016; Wainwright, Stepanian, Reynolds, & Reynolds, 2017) and animal-borne miniaturized loggers for tracking individual birds and bats along their local or migratory movements (e.g. Mora, Ross, Gorsevski, Chowdhury, & Bingman, 2012; Amélineau et al., 2014; Åkesson, Bianco, & Hedenström, 2016; Weller et al., 2016). An important subject in aero-ecology is aerial predation of insects by small specialized birds such as swifts (Apodidae), swallows and martins (Hirundinidae), which has a strong impact on insect population regulation (Kelly, Bridge, Frick, & Chilson, 2013; Helms, Godfrey, Ames, & Bridge, 2016a). However, studies of foraging movements in aerial insectivores are still scarce, because of the technical difficulties in tracking small birds with both fine spatio-temporal resolution and sustained duration. Warrick, Hedrick, Biewener, Crandell, and Tobalske (2016) used sophisticated optical tracking to study low-altitude three-dimensional (3D) foraging manoeuvres in barn swallows, *Hirundo rustica*, at very high resolution (100 Hz) but for short durations (<5 s), whereas, using miniature loggers and postflight diet analysis, Helms et al. (2016a, b) measured foraging in the purple martin, *Progne subis*, for whole flights, but restricted to a single dimension (altitude). Still, studying 3D movements of these small birds while they search for, find and catch prey would be valuable for understanding aerial insectivores' foraging behaviour, that is, how they explore and exploit food resources in airspace.

In numerous species, animals tend to shift from extensive to intensive searching after the detection of a prey item. Extensive

---

* Correspondence: E. de Margerie, CNRS, Laboratoire d'éthologie animale et humaine, Campus de Beaulieu, Bat 25, Porte 304, Avenue de Général Leclerc, Rennes, F-35042, France
E-mail address: emmanuel.demargerie@univ-rennes1.fr (E. de Margerie).

https://doi.org/10.1016/j.anbehav.2017.11.026

searching corresponds to transit, whereas intensive searching leads to a concentration of the searching in the vicinity of the item previously detected. It is often referred to, in 2D space, as area-concentrated (or area-restricted) searching (ACS; e.g. Benhamou, 1992, 1994), and therefore in 3D space can be referred to as volume-concentrated searching (VCS). This shift corresponds to a behavioural adaptation to the heterogeneity of the environment: prey items being often aggregated in patches, the probability of detecting a new prey item close to the previous one is higher than at a random location in the environment. It classically involves increasing the path tortuosity, which allows the predator to remain in close spatial proximity to the location of the previously detected item, and decreasing the speed, which allows it to better detect new, more-or-less cryptic items (Knoppien & Reddingius, 1985). However, a lower speed also results in a lower encounter rate, so that the detection rate, and therefore the foraging efficiency, is not necessarily improved (Benhamou, 1992). Reduced speed usually observed in intensive searching may be more the consequence of the extra time required to handle prey than a means to improve foraging efficiency. In this classical view, where prey are immobile (or move slowly with respect to the predator), shifting from extensive to intensive searching after detecting a prey item is certainly an efficient strategy (Benhamou, 1992, 1994), even when prey are hard to detect (Benhamou & Collet, 2015). However, when prey can move faster to escape predators, it may be preferable to avoid performing ACS. For example, after capturing an item, waders looking for immobile prey perform ACS, whereas others looking for prey able to suddenly hide when disturbed move quickly off the area (Dias, Granadeiro, & Palmeirim, 2009). Only a few studies have focused on shifts from extensive to intensive searching in 3D space, especially in marine mammals (e.g. Le Bras, Jouma'a, Picard, & Guinet, 2016, 2017), and, to our best knowledge, none in aerial species. Yet, the constraints are very different, as the mechanical power required to perform slow flight is very high (Tobalske, 2007), and many flying species are unable to perform sustained hovering flight (i.e. stop movement). For example, in common swifts, wind tunnel experiments show that there is a minimal steady flight speed, in both flapping and gliding flight (Henningsson et al., 2011; Henningsson & Hedenström, 2011). In this context, intensive searching can be expected to rest mainly on higher path tortuosity, with limited change in speed. One should also consider that such aerial predators that hunt in open spaces probably do not need to slow down to detect prey, which should be detectable from a large distance. Thus, in contrast to what occurs with predators looking for hidden prey that can be detected only from a much shorter distance than the patch radius, the perception of the whole patch should facilitate its exploitation. On the other hand, intercepting each prey in flight can require high manoeuvrability, which in animal locomotion is often inversely related to speed (Warrick, 1998; Hedenström & Rosén, 2001; Moore & Biewener, 2015; Clemente & Wilson, 2016). In the present study, we aimed to assess how local flight movements in common swifts reflect their search behaviour. Do common swifts use a VCS foraging strategy in 3D space? If they do so, is aerial VCS based on path tortuosity increase, speed decrease, or both?

Common swifts' level of adaptation to the aerial medium is uncommon. Starting with basic morphology, this species and other Apodidae present a striking allometry with reduced legs (explaining the taxon name) and a very long hand segment (Lack, 1956; Warrick, 1998; Tobalske, 2010). Moreover, their wings can drastically change shape, providing a 'morphing' flight apparatus that combines the performance of several other bird species (Lentink et al., 2007). Their feathers have a rough surface that favours both stiffness and aerodynamism (Lentink & de Kat, 2014; van Bokhorst, de Kat, Elsinga, & Lentink, 2015). Such aerodynamic refinements result in unique aerial behaviour: common swifts are small birds with immense flying skills, which spend most of the day and night flying, sometimes not landing for 10 months (Hedenström et al., 2016). Egg laying, incubation and feeding young (Lack & Lack, 1951) are the sole activities that keep common swifts terrestrial for some of the time for approximately 2 months a year. Hence, they perform most daily activities in mid-air, including foraging, social bonding (Farina, 1988; Henningsson et al., 2010) and probably sleeping, during overnight 'roosting' where the birds settle their flight into the head wind (Bäckman & Alerstam, 2001, 2002; Rattenborg, 2017). Twice daily, common swifts also perform enigmatic high-altitude twilight ascents (Hedenström et al., 2016), possibly to profile atmospheric conditions or to increase their visual range of the ground (Dokter et al., 2013). During migration, common swifts can travel at speeds up to 650 km/day (Åkesson, Klaassen, Holmgren, Fox, & Hedenström, 2012), efficiently orienting their flight according to wind conditions (Karlsson, Henningsson, Bäckman, Hedenström, & Alerstam, 2010; Hedenström & Åkesson, 2017). During the breeding season, nest material collection and mating can also be performed airborne (Lack, 1956; Gory, 1994).

The flight of common swifts has been studied at various temporal and spatial scales, depending on the question addressed and the technique used. Instantaneous biomechanical performance has been measured in wind tunnel experiments using decoys (Lentink et al., 2007) or living swifts (Henningsson, Spedding, Hedenström, 2008, 2011; Henningsson & Hedenström, 2011). In the field, using 3D optical tracking at close range (ca. 8 m), the top speed of common swifts during their fast social flights ('screaming parties') was shown to reach 31 m/s (Henningsson et al., 2010). Tracking-radar-based studies have yielded tracks at the scale of several kilometres, with 0.5 Hz location sampling frequency (Bäckman & Alerstam, 2001, 2002; Henningsson et al., 2009), which provide information on flight speeds and orientation of birds relative to the wind. Similar information has been derived from tracking swifts every few seconds with an 'Ornithodolite' (i.e. a laser rangefinder coupled with a magnetic compass and an inclination sensor; Hedenström & Åkesson, 2017). Weather radar was also used to measure the altitude of swift flocks every 5 min throughout the breeding season and to characterize their twilight ascents (Dokter et al., 2013). Last, a recent technique using miniature light level loggers (GLS) attached to the animal (Åkesson et al., 2012, 2016), possibly coupled with accelerometers to detect landing (Hedenström et al., 2016), was used to track individual annual migration routes from Europe to Africa and back, with a sampling frequency of two locations per day, and a spatial uncertainty in the order of 100 km. Better accuracy and higher sampling frequency would require GPS loggers, which are, however, currently still too heavy for tracking such a small species (ca. 45 g adult body mass; Åkesson et al., 2012). As a result, and even though all these studies make the common swift one of the most scrutinized flying species, we still know little about the spatial behaviour of swifts during their daily local activities.

Recent developments in 3D optical tracking in the field, using several fixed cameras (Theriault et al., 2014; Jackson, Evangelista, Ray, & Hedrick, 2016) or a single camera for rotational stereo-videography (RSV; de Margerie, Simonneau, Caudal, Houdelier, & Lumineau, 2015), make it possible to track flying animals in 3D with a high sampling frequency (>1 Hz), at distances of 10–1000 m depending on the tolerable location error. These noninvasive, tagless optical approaches are promising methods to study flight behaviour, such as tandem flight behaviours in cliff swallows, *Petrochelidon pyrrhonota* (Shelton, Jackson, & Hedrick, 2014) or collective flight behaviour in chimney swifts, *Chaetura pelagica* (Evangelista, Ray, Raja, & Hedrick, 2017). Here we used RSV to track individual common swifts performing aerial foraging flights near their colony during the breeding season. Based on minute(s)-long 3D tracks sampled at 6 Hz, we measured how swifts distribute their presence in 3D space, aiming at identifying their foraging strategy. In addition, with the benefit of a usable image of the bird, we were able to observe the birds' posture to detect signs of prey captures along their tracks.

METHODS

Study Site

We tracked common swifts on the Beaulieu University Campus in Rennes, France, a suburban site offering a mixed landscape of two- to four-floor concrete buildings (where swifts nest in colonies), interspersed with lawns and trees (see Fig. A1). We recorded birds' tracks from a balcony on the second floor of a building, offering a 114° wide panorama. Recording took place in the morning (0900–1300 hours, i.e. before the balcony was under direct sunlight which causes tracking inaccuracy due to heat expansion of the stereo-video device), during six field sessions between 17 June and 9 July 2015. Swifts arrive from their wintering grounds around 10 May in French Brittany (i.e. later than in Italy, but a little sooner than in the U.K.; Lack & Lack, 1951; Sicurella et al., 2015), and were thus recorded about 38–60 days after their arrival, corresponding to the period of nestling growth, when parents make numerous foraging trips from the nest to bring back insects to feed the chicks (Lack & Lack, 1951; Lack, 1956).

Rotational Stereo-Videography (RSV)

RSV is an optical tracking technique based on a set of mirrors which projects a stereo image of the animal on the sensor of a single camera (de Margerie et al., 2015). The analysis of this image provides a measure of the distance to the animal. The rigid assembly of camera plus mirrors can rotate horizontally and vertically on a ground-based tripod and fluid video head. While the operator rotates the device to keep the moving animal's image within the sensor frame, the aiming angles are recorded by angular encoders. The mathematical combination of distance, aiming angles and angular deviation from the optical axis yields a 3D record of the animal's movement. We used an RSV device with a 1 m base length between the lateral mirrors, and 13-bit digital angular encoders (i.e. 0.04° angular resolution). It was the same device as described by de Margerie et al. (2015), except that aluminium stiffeners were added in between the camera and mirrors, for improved rigidity. The device was equipped with a Panasonic DMC-GH4 camera (Osaka, Japan) embedding a 17.3 × 9.7 mm sensor to record 1920 × 1080-pixel frames at 30 Hz, and a Nikon 200 mm f/4 Ai lens (Tokyo, Japan), providing a 5° horizontal field of view. A longer focal length would provide better distance resolution and magnify the image of the bird, but would compromise the ability of the operator to track the bird continuously. To get well exposed, sharp images, we used a 1/1300–1/1000 s shutter speed and f/11 aperture, with ISO 800–1600, depending on available light conditions.

Calibration and Location Error

The distance measure, based on the lateral offset between left and right images of the animal, needs to be calibrated. For this purpose, we recorded seven conspicuous targets (structures on building roofs) located at fixed distances (from 64 to 448 m from the RSV device). Although the true distance to these targets could have been quickly measured in the field with a hand laser rangefinder (as suggested in de Margerie et al., 2015), for optimal accuracy, we used a 3D LIDAR map (Optech Titan, Vegidar survey, LETG COSTEL, Rennes, France) involving a location error of only ±0.15 m. To limit possible calibration drift, we performed a new calibration every hour. At the average tracking distance (ca. 200 m in the present study), the 3D location reconstruction was affected by a random error of ca. 0.8 m. Residual error and drift in the calibration process resulted in additional track scaling error of ca. 1%. As error amount varies with distance, full details on error profiles are given in the Appendix.

Bird Sampling

We attempted to record every individual swift passing through (convenience sampling). We removed from analysis all the numerous tracking videos lasting less than 50 s (as such short footages convey little information on spatial behaviour), thus initially keeping 70 tracks over all six field sessions. However, eight additional videos also had to be removed because the focal bird mainly performed social flight (e.g. pursuits) rather than individual foraging flight. Moreover, most tracks we initially kept had missing locations, due to difficulty in keeping the bird within the viewfinder or obstruction by the environment (e.g. lateral walls of the balcony, tree). Short missing track segments of up to 1.5 s were interpolated (using a spline smoothing process; see below). Longer ones were left as transient intermissions in the analysed tracks. However, four tracks involving more than 10% of missing locations and lacking a tracking segment of at least 50 s, and another involving a bird moving too far (> 500 m), were also removed from analysis. The resulting data set hence comprised 57 flight tracks, with a mean duration of 98 s (range 50–359 s), totalling 5559 s of tracking (including 111 s of transient intermissions distributed among 14 tracks). Although these remaining 57 tracks mainly concerned individual flights, transitory social interactions between the focal bird and another bird, such as short pursuits or collision avoidances, were often observed. We also considered steep dives towards the colony as a socially motivated movement. We noted which video frames were potentially affected, to later test whether these transitory social interactions (totalling 260 s of flight duration, distributed among 30 tracks) could have affected our results on foraging flight behaviour.

Track Processing

We processed stereo videos and angular records with Matlab software (Mathworks, Natick, MA, U.S.A.). As the average flight speed of the common swift is near 9 m/s (Bäckman & Alerstam, 2001; Henningsson et al., 2009; Henningsson & Hedenström, 2011), we subsampled 30 Hz video frames at 6 Hz, assuming one location about every 1.5 m was enough to resolve every significant turn in the flight paths. It is also worth noting that, given the location error, a higher frequency would not necessarily have resulted in more accurate records (see de Margerie et al., 2015). For digitizing the bird's locations in the video frames, the pixel at the centroid of the bird's silhouette in the left half of each video frame was automatically selected as the left point of interest (POI). All left POIs were visually inspected and corrected when needed (e.g. the POI was manually moved to the centroid of the bird's body if initially placed on the bird's wing). Automated normalized cross-correlation between a 41 × 41-pixel area around the left POI and the right image was used to find the corresponding right POI. Subsequent steps to extract the 3D track consisted of computing the distance based on the calibration reference, synchronizing it with angular records (joint azimuth and inclination, and angular deviation from the optical axis), and converting from spherical to Cartesian coordinates (see de Margerie et al., 2015 for details). As the resulting raw 3D tracks included significant levels of noise due to random location errors, we smoothed them using automated spline smoothing (Garcia, 2010), which also enabled us to interpolate short ($\leq$1.5 s, i.e. $\leq$9 locations) missing bouts. We checked that smoothing did not alter the general shape of the track, i.e. that flight turns were not suppressed or displaced (see Fig. A3). As birds fly in a moving medium (Shepard, Ross, & Portugal, 2016a) and their aerial prey, for the most part, drift with the wind (Geerts & Miao, 2005; Wainwright et al., 2017), we measured wind velocity (speed and direction) in the field by releasing a helium-filled balloon every hour and tracking it with the RSV device (mean wind speed 2.83 m/s, range 0.38–8.39). Then, we derived air mass-based tracks by subtracting the horizontal wind velocity (measured at the appropriate altitude) from the initial ground-based recorded tracks (see Bäckman & Alerstam, 2001 or Girard, Sudre, Benhamou, Roos, & Luschi, 2006 for details). However, note that vertical air movements such as thermal updrafts, which are too variable to be reliably measured with intermittent balloon launches, were not corrected: only the horizontal velocity of the balloon was considered.

Residence Time Computation

For 2D movements, an efficient way to detect ACS is to compute the residence time (RT) within a virtual circle running along the path (Barraquand & Benhamou, 2008). This approach can be easily applied to 3D movements to detect VCS by considering a virtual sphere instead of a virtual circle (Fig. 1). Each location along the flight track has an associated RT value, equal to the sum of the durations of the track portions occurring within a distance ρ (corresponding to the sphere radius) of this location. RT is therefore equal to the current crossing duration (that is, the difference between the first passage times at the sphere surface in the forward and backward directions), plus the durations of some possible additional backward and forward crossings, to get a more reliable signal. Note that in contrast to the current crossing, additional crossings need not move through the sphere's centre. When studying long-term recursive movements in 2D, an upper threshold for the time the animal is allowed to spend outside the circle before re-entering it has to be set to exclude possible crossings linked to new visits to the area (Benhamou & Riotte-Lambert, 2012). As only short tracks were involved in the present study, we chose to take all sphere crossings into account. As a result, here RT is simply equal to the total time spent by the bird inside a sphere centred on the current location. Passage times through the surface of the sphere were determined through linear interpolation based on the coordinates of the inside and outside locations recorded just before and after the passage (see details in the Appendix).

The sphere radius ρ must be large enough to smooth random variations and thus obtain a good contrast between extensive and intensive searching phases, but nevertheless small enough to keep a good resolution in the movement analysis. After some trials and errors, it appeared that the RT signal was more reliable if the sphere could fully encompass the ‘loops’ in the flight paths (i.e. closed path in *x/y* view). Having observed that 90% of loops had a diameter of less than 30 m we set ρ to 30 m. To decompose RT into its tortuosity and speed components, we also computed the ‘residence length’ RL associated with every location, that is, the overall length of all crossings within the sphere centred on the location in question. The mean speed in the sphere V associated with any location was then given by $V = \mathrm{RL/RT}$. The minimal theoretical value for RL is equal to the sphere's diameter (60 m). An expected edge effect near the ends of tracks that could cause RL to be $<$ 60 m was corrected by increasing RL up to 60 m for these locations, and RT was increased in the same proportion, such that V in the sphere was unchanged by the correction.

Bird Posture and Prey Captures

As RSV is based on a longer focal length than most fixed camera tracking techniques (e.g. Theriault et al., 2014), the resulting images benefit from a relatively higher magnification, and can convey interesting complementary information on bird behaviour while it is tracked. Swift images corresponded to a ca. 15–100-pixel-long silhouette depending on distance, on which we could observe the bird's posture, that is, the general relative positions of body, wings, tail and head. By carefully inspecting 30 Hz videos, we noticed that swifts frequently adopted ‘atypical postures’ (APs), characterized by an extended head, often associated with partially retracted wings,

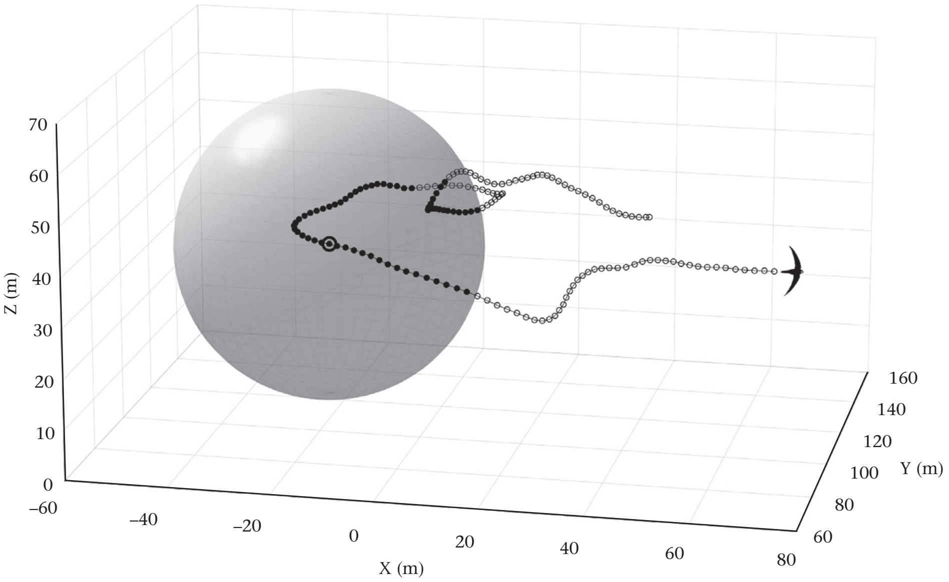

Figure 1. Residence time (RT) computed along a 3D flight track. For each location, RT is computed as the total time spent by the bird inside a virtual sphere of radius $\rho = 30$ m, centred on this location (larger circle). Recorded locations included in the sphere are filled in black. In this example, the bird crosses the sphere twice, and RT is equal to the sum of the two crossing durations (computed through interpolation of entrance and exit times based on the closest recorded locations). Note that the bird is not drawn to scale (ca. ×20).

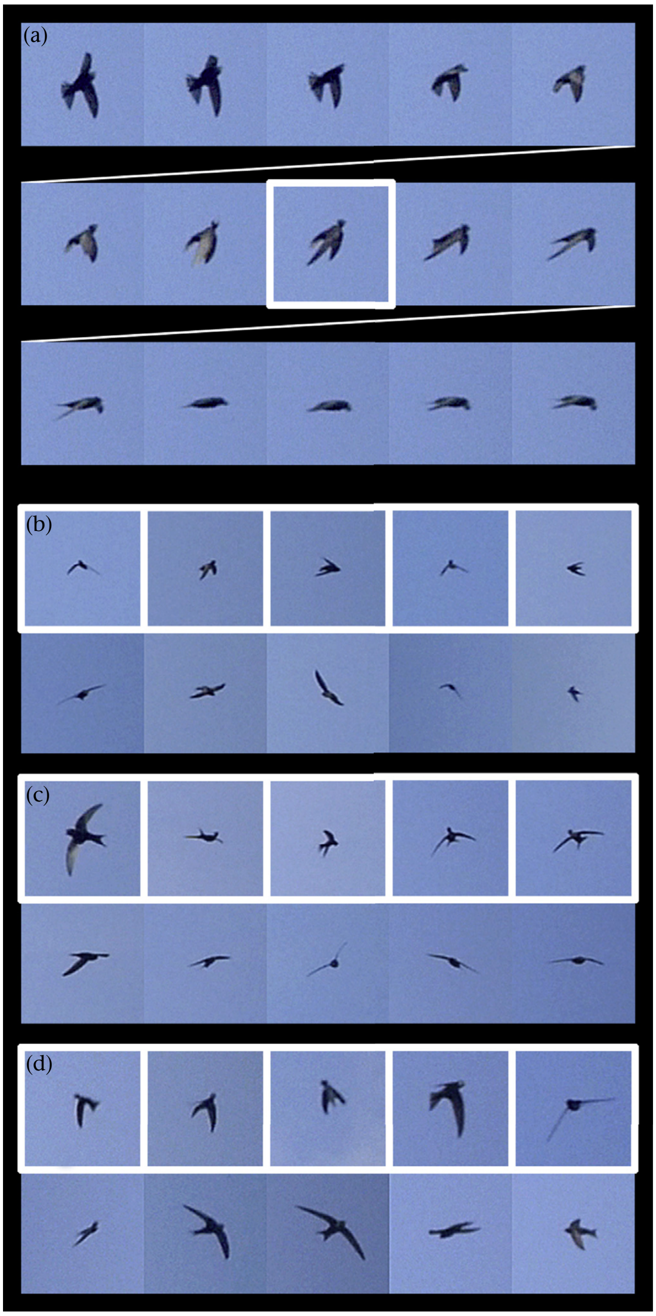

Figure 2. Atypical postures (APs) during common swift flight. Each square image shows a 100 × 100-pixel window extracted from an RSV video frame. (a) Fifteen successive frames (0.5 s total duration) show the bird extending its head and partially retracting its wings, until attaining the AP climax (white bordered frame), and then returning to a more typical flight posture. (b–d) The first five APs from three individual bird-tracking videos. Underneath each AP (white bordered frames), an image of the same bird taken 5 s after the AP shows a typical flight posture for comparison.

that is, strong negative dihedral and backward sweep angles (Fig. 2). The most striking point was that APs were very transitory, the bird quickly returning to a typical flight posture with extended wings and retracted head. Although the magnification was too low to enable us to discern direct evidence of prey intake (e.g. gape opening, insect trace), we assumed that APs mostly reflected prey captures, or at least attempts thereof. Similar criteria (e.g. neck extension) have been used to detect insect captures in aerial insectivores (Warrick, 1998). We noted when each AP occurred by identifying the frame in which the climax AP occurred in the 30 Hz video (Fig. 2a) and assigned it to the nearest 3D location in the 6 Hz track, irrespective of any consideration about flight path shape or speed. Then, for each recorded track location, we estimated the local frequency F of the (attempts at) prey captures by dividing the number of APs (n_{AP}) identified along the movement bouts included in the sphere by the corresponding RT value: $F = n_{AP}/\text{RT}$.

Statistical Analysis

Correlation between RT and other variables (e.g. RL, V, F) was measured individually for each track using the Pearson correlation coefficient r across all locations in the track. Because of the high serial correlation in track locations, the significance of r was not tested at the individual track level. Instead, we used a one-sample two-tailed Student t test to detect whether the mean r value across $N = 57$ tracks was significantly different from zero.

RESULTS

RT Distribution and Decomposition

For all 57 tracks pooled, RT ranged from 2.5 s to 76.2 s (Fig. 3). RTs in the [5–10] s range were the most frequent, one-third of locations. Spatially, this corresponded to single, low-tortuosity transit through the sphere. On the extreme left side, RTs < 5 s were much less frequent (<5%). On the right side, RTs in the [10–15] s range reflected moderate increase in presence, the bird often performing a single ‘loop’ (i.e. closed path in x/y view) whereas RTs > 15 s, corresponding to more intense presence, involved multiple loops and multiple crossings through the sphere. For these large RT values, the frequency of occurrence decreased with increasing RT, RTs > 60 s being observed for less than 1% of locations. Fig. 4 illustrates diverse examples of common swift flight tracks with superimposed RT values. While some tracks corresponded only to a transit flight (RT < 10 s for every location, Fig. 4a), most involved zones of concentrated presence, corresponding to RT > 10 s (Fig. 4b–e), interspersed in between transit bouts. The level of concentration was variable, with maximal RT values reaching 30.7, 38.2, 55.8 and 58.6 s in Fig. 4b–e, respectively. Fig. 5 shows how RL, V and RT were related. RTs < 5 s corresponded to straight paths (RL = 61.4 ± 1.9 m; mean ± SD), just slightly longer than the minimum possible value set by the sphere

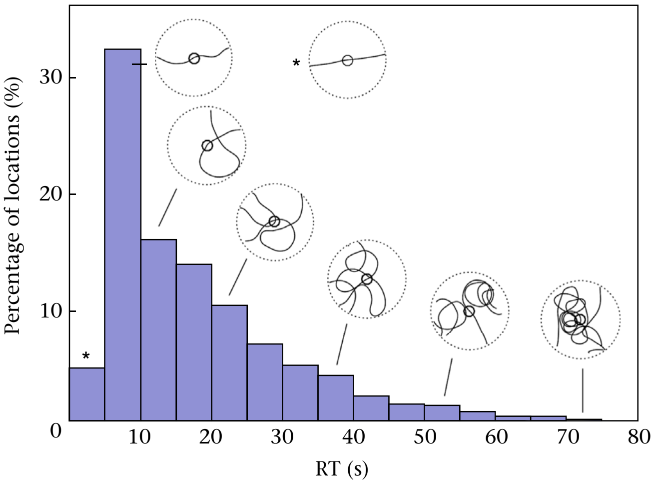

Figure 3. Residence time (RT) distribution for all track locations. Examples of track bouts crossing the sphere are shown in top view (x/y projection).

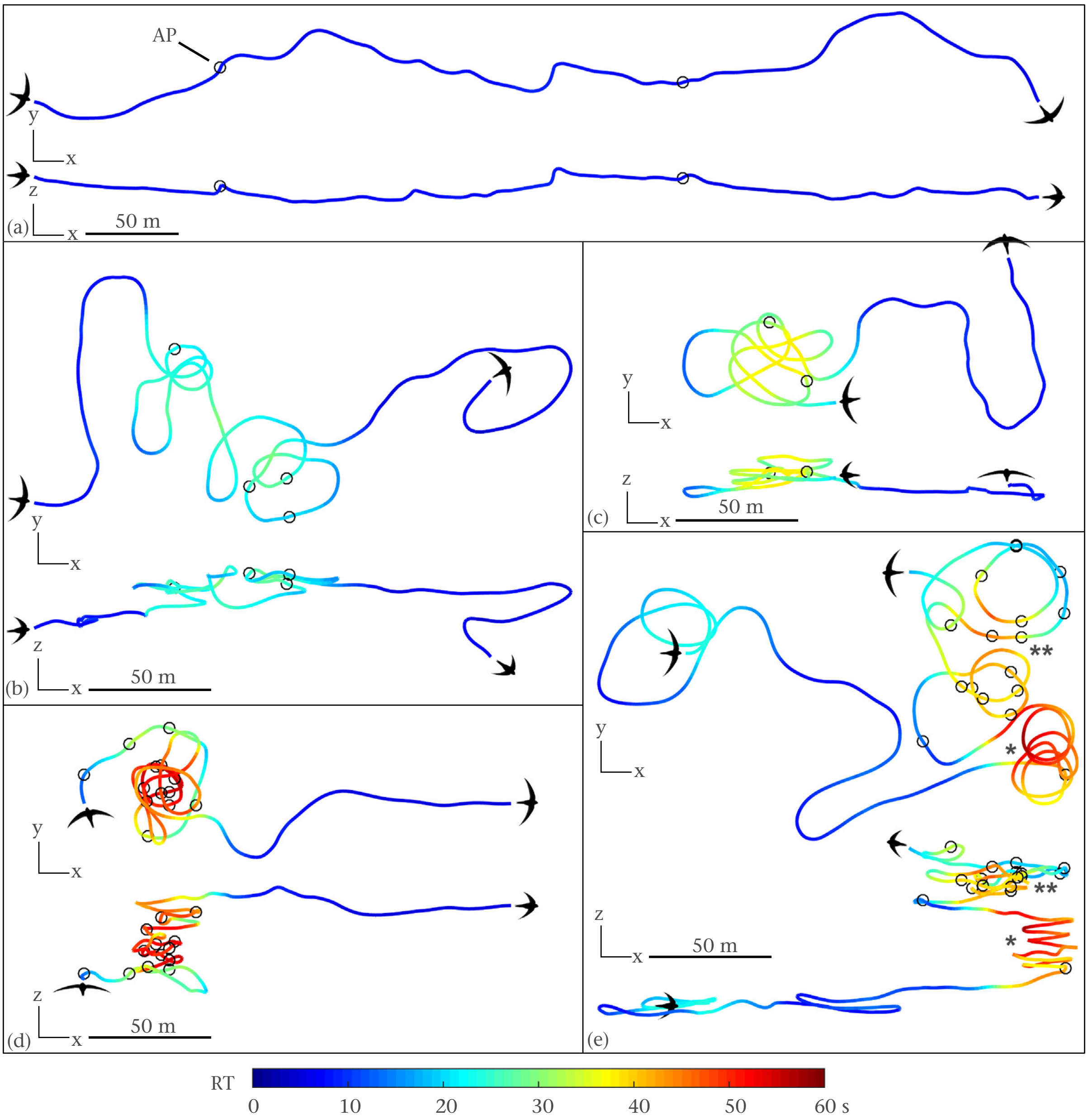

Figure 4. Common swifts' 3D flight tracks. (a–e) The five tracks illustrated here in top view (*x*/*y*) and side view (*x*/*z*) show varying RT values (colour scale). Black circles indicate detected atypical flight postures (APs). * and ** indicate specific track segments discussed in the main text. Durations were 61, 83, 58, 72 and 175 s, and lengths 613, 868, 603, 610 and 1396 m, for tracks a–e, respectively. Note that tracks b–e are shown at the same scale, but track a was scaled down (×0.75) to fit in the figure. The bird drawings indicate flight direction and are not to scale (ca. ×40).

diameter (60 m), associated with high speed (14.1 ± 1.9 m/s). The modal RT of [5–10] s was associated with a mean RL of 70.1 ± 12.5 m, and a mean speed of 10.1 ± 1.3 m/s. Higher RT values were due to an increase in RL, up to 580.6 ± 2.1 m for RTs > 75 s, and a moderate reduction in mean flight speed, down to a minimum of 7.1 ± 0.4 m/s for RTs in the range [65–70] s. Hence swifts tended to increase RT mainly by following more tortuous paths (times 8 compared to modal RT), but also by slowing down a little bit (times 0.7 compared to modal RT). The mean correlations between RL and RT and between *V* and RT, computed independently for each of the 57 individual tracks, were significantly different from 0 in both cases (*t* test: $t_{56} = 189$ and $t_{56} = -13.8$, respectively, $P < 0.0001$), as expected as RL and *V* are components of RT. However, the mean ± SD correlation obtained between RL and RT ($r = 0.97 \pm 0.04$) means that, on average, more than 90% of the variance in RT was explained by variance in RL whereas the mean value obtained between *V* and RT ($r = -0.55 \pm 0.30$) means that only 30% of the variance in RT was explained by variations in *V* (the percentages did not sum to 100 because of some interaction between RL and *V*).

RT and Putative Prey Captures

We identified 316 APs over the cumulated tracking duration, corresponding to an overall mean frequency of 0.06 Hz (one AP every 17 s on average). Fig. 6 shows that *F* increased from 0.02 ± 0.07 Hz for fast transit (RTs < 5 s) up to 0.20 ± 0.05 Hz for RTs in the range [65–70] s, representing about one putative prey

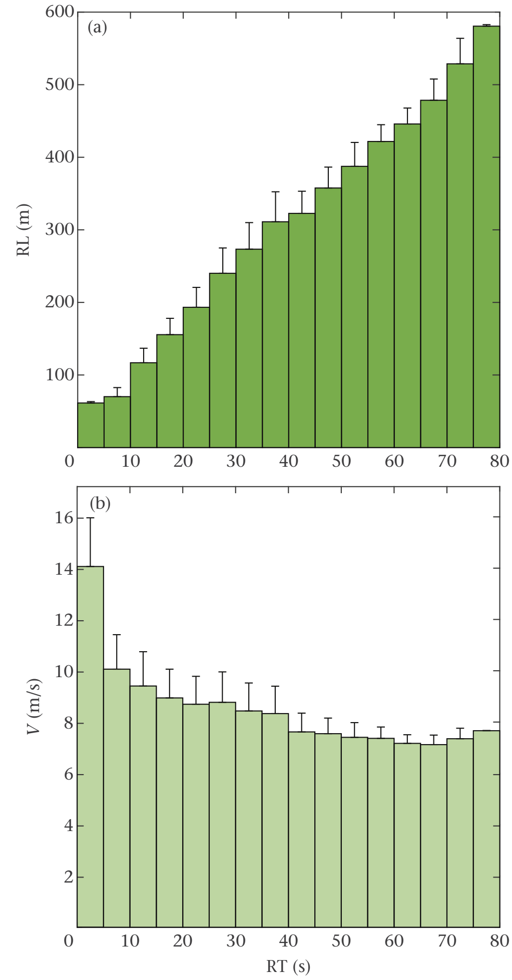

Figure 5. Residence time (RT) components as a function of RT. (a) Residence length (RL). (b) Mean speed (V). Each bar shows the mean for all track locations with the RT value included in each 5 s-wide bin. Error bars represent SD.

capture (or attempt) every 5 s. For the 50 tracks where APs were identified, we computed the correlation coefficient between F and RT. The mean value ($r = 0.27 \pm 0.33$) was significantly positive ($t_{49} = 5.69$, $P < 0.0001$), even though this linear relationship can on average explain only 7% of the total variance of RT. It is worth noting that the correlation level varied to a large extent from one track to the other (range −0.28 to 0.90). For instance, in Fig. 4a–e, the r values between RT and F were 0.16, 0.60, 0.87, 0.67 and 0.15, respectively. APs were not necessarily linked to VCS. Indeed, we observed several APs during transit flight (e.g. see Fig. 4a). Over the whole data set, track locations with RTs < 10 s (encompassing fast- and normal-speed transit flight, involving 38% of locations) contained as much as 22% of detected APs, which therefore did not trigger, or at least were not associated with, VCS behaviour. We also observed a few examples of high RT with few or no associated APs. For example, the track illustrated on Fig. 4e showed a globally loose association between RT and F ($r = 0.15$ for the whole track). A phase of this track (marked **) was characterized by both high RT values (in the [30–40 s] range) and frequent APs, but a previous phase (marked *) was characterized by an even higher RT (ca. 50 s) without frequent APs. In this previous phase, the smooth spiralling path shape suggests pure thermal soaring flight, showing that high RTs may not necessarily correspond to VCS. To investigate this point, we measured the mean vertical speed in the sphere (V_z) for every location. Fig. 7 suggests that there was a positive association between V_z and RT. Low RT values (<10 s) were usually associated with negative V_z, indicating a descending flight path, while high RT values were associated with positive V_z up to about 0.5 m/s. The correlation between RT and V_z obtained for each track was significantly larger than 0 (mean $r = 0.25 \pm 0.28$, $t_{56} = 6.78$, $P < 0.0001$). Hence, high RTs were likely to reflect VCS as well as thermal soaring, and maybe associations of both. A measure of the direct covariation between V_z and F (i.e. testing for more frequent captures in thermals) revealed only a weak positive correlation (mean $r = 0.13 \pm 0.37$, $t_{49} = 2.58$, $P = 0.013$), indicating that the stronger correlation between RT and F (Fig. 6) cannot be a spurious outcome of a strong association between RT and V_z on the one hand and V_z and F on the other.

Sensitivity Analysis

We tested whether the above-reported correlations between RT and RL, V, F and V_z were sensitive to (1) a different sphere radius and (2) the occurrence of transitory social interactions during flight. We recomputed the correlations for sphere radii of 20 m and 40 m instead of 30 m, and keeping a radius of 30 m, for a track data set

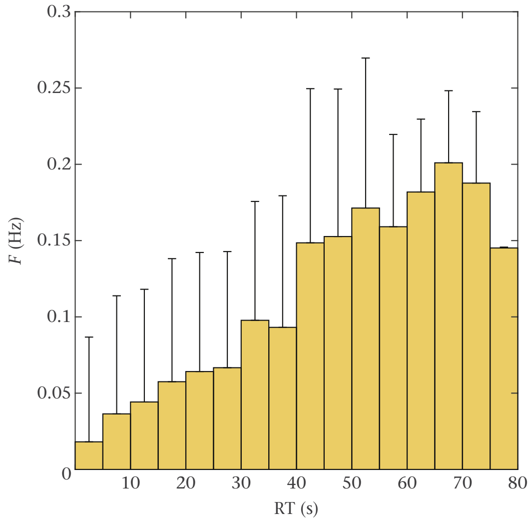

Figure 6. Estimated local prey capture frequency (F) as a function of residence time RT. Each bar shows the mean for all track locations with the RT value included in each 5 s-wide bin. Error bars represent SD.

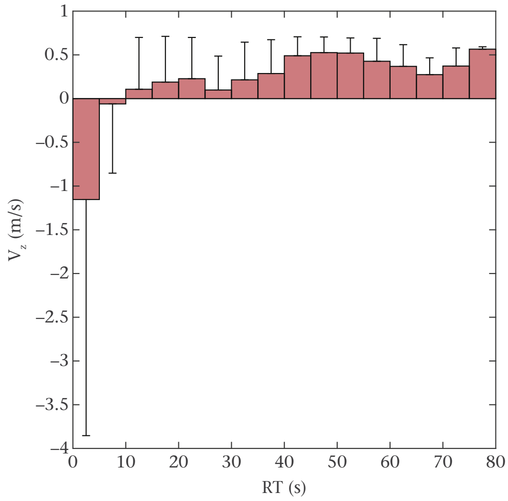

Figure 7. Vertical speed in the sphere (V_z) as a function of residence time RT. Each bar shows the mean for all track locations with the RT value included in each 5 s-wide bin. Error bars represent SD.

with short phases of social interactions removed. None of these modifications affected our results (see Table A1).

DISCUSSION

To our knowledge, the present study is a first attempt at analysing aerial foraging in an insectivorous bird with both a high-enough sampling frequency to resolve individual turns in the flight path and enough duration to observe how successive flight manoeuvres are carried out in time and space. Our study certainly suffers from some methodological limitations. In particular, although the convenience sampling scheme we used is efficient for extracting numerous tracks during each field session, individual birds were not identified, and therefore might have been recorded several times. With a rough estimation of about 300 birds nesting in or near our study area, pseudoreplication did certainly occur but should be limited to a few tracks in our sample. Another limitation with optical tracking is the strong effect of distance on bird detection and tracking accuracy, which constrains the size of the study area, and hence the tracking duration. Despite such limitations, our study clearly showed that the residence time (RT), that is, the time spent in the vicinity of any given track location, provides an interesting tool for inferring the behaviour along the track. It was shown to vary up to 30 times between the parts corresponding to straight and fast movements and those corresponding to slower and tortuous ones. Interestingly, larger RT values were very often, although not systematically, obtained with larger frequencies, *F*, of putative prey captures (APs). The positive correlation between RT and *F* suggests that common swifts tend to concentrate their presence in the vicinity of previous prey encounters, that is, to improve their foraging efficiency by performing VCS. Our results show a gradual increase in RT from transit to very concentrated presence (Fig. 6), suggesting that swifts adapt their foraging behaviour to the prey density.

We observed that VCS was performed mainly by increasing flight length (RL) in the sphere, and therefore path tortuosity, even though VCS also involved a moderate decrease in flight speed (*V*; Fig. 5), from an average 10.1 m/s for modal transit flight down to near 7.1 m/s during intense VCS. A basic prediction, relying on gliding flight mechanics only, is that swifts should transit between prey patches at speeds providing a shallow glide angle, and shift to a speed that minimizes height loss per time unit when returning to VCS inside a prey patch. Henningsson and Hedenström (2011) reported that a common swift gliding in a wind tunnel had a speed of best glide of 9.5 m/s and a speed of minimum sink of 8.1 m/s. Moreover, the bird was capable of gliding at 7 m/s with marginally increased sink, but was not capable of steadily gliding at lower speeds. This suggests that the speed decrease we observed during VCS would simply represent the optimal behaviour for aerodynamic performance, with minimal cost for the bird. However, our swifts also performed some flapping flight (about 20% of the time; de Margerie & Pichot, n.d.), during which they can further lower flight speed (down to 5.7 m/s, Henningsson et al., 2011), but at a high mechanical and metabolic cost (Tobalske, 2007). The picture is even more complex as the swifts we tracked performed a lot of horizontal and vertical turning, during which the balance of aerodynamical forces (e.g. Warrick, 1998) is different from forward, steady flight in a wind tunnel. Hence measuring the possible cost of slow, manoeuvring flight during VCS is complex. It needs a precise, per-track analysis of instantaneous speeds, accelerations and gliding/flapping behaviour, which is beyond the scope of the present 'macroscopic' study (we intend to do this in the future). Nevertheless, in contrast to what occurs with terrestrial or aquatic predators, birds acting as aerial predators cannot stop their movement without performing a very costly hovering flapping flight (Tobalske, 2007). For numerous bird species, including the common swift, hovering is simply too costly to be sustained (Henningsson et al., 2011). For a flying common swift, the movement coming closest to remaining in the same spot is probably a circling flight at about 6–7 m/s. This mechanical constraint on minimum speed probably explains why swifts must rely on such drastic increase in path tortuosity to remain in the vicinity of a prey patch. More generally, and beyond the case of the common swift, the relationship between movement speed and movement cost (per time unit) is U-shaped (Tobalske, 2007) in flying vertebrates, whereas it increases monotonically for terrestrial and aquatic movement (Bennett, 1985). This point should be kept in mind when studying or predicting the movement of non-buoyant flying species.

The correlation between RT and *F*, although of similar strength to previous reports for 2D search (Dias et al., 2009), is rather low, which may arise from various causes. Birds may have performed APs only when they were able to come close enough to a prey item to be almost sure to catch it, and thus could increase RT by passing numerous times through a prey patch without increasing the number of APs in the same proportion (or even without any AP if the bird finally gives up and stops VCS). Furthermore, as APs are rare (5.5 APs per track on average) and discrete events, the measure of *F* along a single track cannot be as smooth as the measure of RT, probably resulting in drastic variations in the correlation between RT and *F*. Prey capture without VCS may also occur because the diet of the common swift is very diverse (Gory, 2008), made up of arthropods from various taxa: mainly Hemiptera, Diptera, Coleoptera, Hymenoptera, but also Lepidoptera, Odonata and Arachnida depending on the foraging location and season. The size of these prey can vary by more than one order of magnitude, and smaller prey are likely to 'float around' and drift in patches (Geerts & Miao, 2005; Wainwright et al., 2017) for which VCS would be adaptive, but larger, faster prey (e.g. wasps) are less likely to form patches (at least at the present spatio-temporal scale), so that the capture of one isolated individual might not need further spatial search in the vicinity. Hence, the casual occurrence of APs not associated with high RT may reflect the diversity of aerial prey behaviours. Last, although we are confident that a majority of detected APs reflect actual or attempted prey captures, we cannot rule out that some of these in-flight postures were in fact expressions of other behaviours such as preening or social display (Lack, 1956; Rothgänger & Rothgänger, 1973). In the present study, we assumed that an extended head, often associated with partly retracted wings, indicates prey capture attempts, in agreement with previous observations in other aerial insectivores (Warrick, 1998). However, common swifts must perform almost all activities aerially, including social and maintenance behaviours, so that our assumption about APs should be considered preliminary. It is also probable that some APs at large tracking distances were not detected, and that some prey captures required only gape opening, without associated APs.

Like many other bird species, swifts can soar in thermal updrafts to gain height economically (Lack, 1956; Hedenström et al., 2016). Hence high RT may reflect not only VCS but also travel cost reduction movements where the bird remains circling in a rising air mass to gain height (as discussed previously for Fig. 4e*). In contrast to steady horizontal-wind-driven updrafts above obstacles such as hills or buildings, which can be reliably modelled from terrain profile and wind speed measurement (e.g. Shepard, Williamson, & Windsor, 2016b), fine-scale thermal updrafts are nonsteady convective flows, involving complex field measurements and models (see Reddy, Celani, Sejnowski, & Vergassola, 2016 for a recent simulation approach). Here, all we could reasonably consider was the mean vertical speed V_z of swifts, assuming that prolonged positive values reflected flight in a thermal updraft. RT was correlated with both F and V_z, but F and V_z were only weakly associated. Consequently, high RT can correspond to level-flight VCS (high F, low V_z; Fig. 4b and c), thermal soaring without foraging ($F = 0$, $V_z >> 0$; Fig. 4e*) or VCS in thermal updraft (high F, $V_z >> 0$; Fig. 4d, e**). It is worth noting that the third possibility was frequent among the tracks we recorded, resulting in some ambiguity about the bird's primary motivation (catching prey or gaining free height). Interestingly, several tracks revealed that after gaining height and catching prey in a thermal, the bird would suddenly adopt a fast, steeply descending path (see Fig. A6), presumably directed towards the bird's nest. In doing so, the potential energy previously gained was quickly 'wasted', that is, it was not used to travel further horizontally. This behaviour suggests that the primary motivation during the thermal ascent was indeed foraging, and that, in this case, thermal flight was not a means to reduce travel costs, unlike along commuting tracks or migration (e.g. Shepard, Lambertucci, Vallmitjana, & Wilson, 2011; Hedenström et al., 2016). Instead, spiralling in a thermal updraft can simply reflect the bird's attempts to remain in the vicinity of a patch of prey floating in up-drafting air. In other words, in the specific context of aerial foraging near the breeding colony in which our study took place, a significant part of the vertical movements of swifts could be an edge effect of prey patchiness being partly structured by thermal currents (Geerts & Miao, 2005; Wainwright et al., 2017).

Acknowledgments

We thank S. Lumineau, C. Houdelier, I. George, M. Trabalon and F. Pittet (DEPP research team, Laboratoire d'Ethologie Animale et Humaine) for endorsing the development of the swift flight study. We thank F. Nassur and S. Louazon (Laboratoire d'Ethologie Animale et Humaine) for technical support in the field. We thank J. Nabucet and S. Croci (Climat et Occupation du Sol par Télédétection, LETG, Rennes, France) for kindly providing the LIDAR map used for calibration. We also thank C. Baczkowski (AST35) for providing access to property for swift filming. Finally, we thank two anonymous referees for their comments and Angela Turner for her keen editing of our manuscript. RT and RL along the 3D tracks were computed using a Pascal custom-written program that runs thanks to the Freepascal compiler (www.freepascal.org). This work was supported by the base funding from the authors' institutions. The authors declare no conflict of interest.

References

Åkesson, S., Bianco, G., & Hedenström, A. (2016). Negotiating an ecological barrier: Crossing the sahara in relation to winds by common swifts. *Philosophical Transactions of the Royal Society B: Biological Sciences, 371*(1704). https://doi.org/10.1098/rstb.2015.0393, 20150393.

Åkesson, S., Klaassen, R., Holmgren, J., Fox, J. W., & Hedenström, A. (2012). Migration routes and strategies in a highly aerial migrant, the common swift *Apus apus*, revealed by light-level geolocators. *PLoS One, 7*(7), e41195. https://doi.org/10.1371/journal.pone.0041195.

Amélineau, F., Péron, C., Lescroël, A., Authier, M., Provost, P., & Grémillet, D. (2014). Windscape and tortuosity shape the flight costs of northern gannets. *The Journal of Experimental Biology, 217*(6), 876–885. https://doi.org/10.1242/jeb.097915.

Bäckman, J., & Alerstam, T. (2001). Confronting the winds: Orientation and flight behaviour of roosting swifts, *Apus apus*. *Proceedings of the Royal Society B: Biological Sciences, 268*(1471), 1081–1087. https://doi.org/10.1098/rspb.2001.1622.

Bäckman, J., & Alerstam, T. (2002). Harmonic oscillatory orientation relative to the wind in nocturnal roosting flights of the swift *Apus apus*. *The Journal of Experimental Biology, 205*(7), 905–910.

Barraquand, F., & Benhamou, S. (2008). Animal movements in heterogeneous landscapes: Identifying profitable places and homogeneous movement bouts. *Ecology, 89*(12), 3336–3348.

Benhamou, S. (1992). Efficiency of area-concentrated searching behaviour in a continuous patchy environment. *Journal of Theoretical Biology, 159*(1), 67–81. https://doi.org/10.1016/S0022-5193(05)80768-4.

Benhamou, S. (1994). Spatial memory and searching efficiency. *Animal Behaviour, 47*(6), 1423–1433. https://doi.org/10.1006/anbe.1994.1189.

Benhamou, S., & Collet, J. (2015). Ultimate failure of the Lévy Foraging Hypothesis: Two-scale searching strategies outperform scale-free ones even when prey are scarce and cryptic. *Journal of Theoretical Biology, 387*, 221–227. https://doi.org/10.1016/j.jtbi.2015.09.034.

Benhamou, S., & Riotte-Lambert, L. (2012). Beyond the utilization distribution: Identifying home range areas that are intensively exploited or repeatedly visited. *Ecological Modelling, 227*, 112–116. https://doi.org/10.1016/j.ecolmodel.2011.12.015.

Bennett, A. F. (1985). Energetics and locomotion. In M. Hildebrand, D. Bramble, K. Liem, & D. Wake (Eds.), *Functional Vertebrate Morphology* (pp. 173–184). Cambridge, MA: Harvard University Press.

van Bokhorst, E., de Kat, R., Elsinga, G. E., & Lentink, D. (2015). Feather roughness reduces flow separation during low Reynolds number glides of swifts. *The Journal of Experimental Biology, 218*(20), 3179–3191. https://doi.org/10.1242/jeb.121426.

Chapman, J. W., Nilsson, C., Lim, K. S., Bäckman, J., Reynolds, D. R., Alerstam, T., et al. (2015). Detection of flow direction in high-flying insect and songbird migrants. *Current Biology, 25*(17), R751–R752. https://doi.org/10.1016/j.cub.2015.07.074.

Clemente, C. J., & Wilson, R. S. (2016). Speed and maneuverability jointly determine escape success: Exploring the functional bases of escape performance using simulated games. *Behavioral Ecology, 27*(1), 45–54. https://doi.org/10.1093/beheco/arv080.

de Margerie, E., & Pichot, C. (n.d.). [*Dataset on natural flight gaits of common swifts*]. In preparation.

de Margerie, E., Simonneau, M., Caudal, J.-P., Houdelier, C., & Lumineau, S. (2015). 3D tracking of animals in the field using rotational stereo videography. *The Journal of Experimental Biology, 218*(16), 2496–2504. https://doi.org/10.1242/jeb.118422.

Dias, M. P., Granadeiro, J. P., & Palmeirim, J. M. (2009). Searching behaviour of foraging waders: Does feeding success influence their walking? *Animal Behaviour, 77*(5), 1203–1209. https://doi.org/10.1016/j.anbehav.2009.02.002.

Diehl, R. H. (2013). The airspace is habitat. *Trends in Ecology & Evolution, 28*(7), 377–379. https://doi.org/10.1016/j.tree.2013.02.015.

Dokter, A. M., Åkesson, S., Beekhuis, H., Bouten, W., Buurma, L., van Gasteren, H., et al. (2013). Twilight ascents by common swifts, *Apus apus*, at dawn and dusk: Acquisition of orientation cues? *Animal Behaviour, 85*(3), 545–552. https://doi.org/10.1016/j.anbehav.2012.12.006.

Evangelista, D. J., Ray, D. D., Raja, S. K., & Hedrick, T. L. (2017). Three-dimensional trajectories and network analyses of group behaviour within chimney swift flocks during approaches to the roost. *Proceedings of the Royal Society B: Biological Sciences, 284*(1849). https://doi.org/10.1098/rspb.2016.2602.

Farina, A. (1988). Observations on the Swift's *Apus Apus* (l.) social flights at the breeding sites. *Monitore Zoologico Italiano, 22*(3), 255–261. https://doi.org/10.1080/00269786.1988.10736557.

Frick, W. F., Stepanian, P. M., Kelly, J. F., Howard, K. W., Kuster, C. M., Kunz, T. H., et al. (2012). Climate and weather impact timing of emergence of bats. *PLoS One, 7*(8), e42737. https://doi.org/10.1371/journal.pone.0042737.

Garcia, D. (2010). Robust smoothing of gridded data in one and higher dimensions with missing values. *Computational Statistics & Data Analysis, 54*(4), 1167–1178. https://doi.org/10.1016/j.csda.2009.09.020.

Geerts, B., & Miao, Q. (2005). Airborne radar observations of the flight behavior of small insects in the atmospheric convective boundary layer. *Environmental Entomology, 34*(2), 361–377. https://doi.org/10.1603/0046-225X-34.2.361.

Girard, C., Sudre, J., Benhamou, S., Roos, D., & Luschi, P. (2006). Homing in green turtles *Chelonia mydas*: Oceanic currents act as a constraint rather than as an information source. *Marine Ecology Progress Series, 322*, 281–289. https://doi.org/10.3354/meps322281.

Gory, G. (1994). Recherche et utilisation des matériaux nécessaires à la construction de nid du martinet noir *Apus apus*. *Alauda, 62*(2), 117–122.

Gory, G. (2008). Diet of the common swift (*Apus apus*) in the mediterranean region. *Revue d'Ecologie (Terre et Vie), 63*, 251–260.

Hedenström, A., & Åkesson, S. (2017). Adaptive airspeed adjustment and compensation for wind drift in the common swift: Differences between day and night. *Animal Behaviour, 127*, 117–123. https://doi.org/10.1016/j.anbehav.2017.03.010.

Hedenström, A., Norevik, G., Warfvinge, K., Andersson, A., Bäckman, J., & Åkesson, S. (2016). Annual 10-month aerial life phase in the common swift *Apus apus*. *Current Biology, 26*(22), 3066–3070. https://doi.org/10.1016/j.cub.2016.09.014.

Hedenström, A., & Rosén, M. (2001). Predator versus prey: On aerial hunting and escape strategies in birds. *Behavioral Ecology, 12*(2), 150–156. https://doi.org/10.1093/beheco/12.2.150.

Helms, J. A., Godfrey, A. P., Ames, T., & Bridge, E. S. (2016a). Are invasive fire ants kept in check by native aerial insectivores? *Biology Letters, 12*(5). https://doi.org/10.1098/rsbl.2016.0059.

Helms, J. A., Godfrey, A. P., Ames, T., & Bridge, E. S. (2016b). Predator foraging altitudes reveal the structure of aerial insect communities. *Scientific Reports, 6*. https://doi.org/10.1038/srep28670, 28670.

Henningsson, P., & Hedenström, A. (2011). Aerodynamics of gliding flight in common swifts. *The Journal of Experimental Biology, 214*(3), 382–393. https://doi.org/10.1242/jeb.050609.

Henningsson, P., Johansson, L. C., & Hedenström, A. (2010). How swift are swifts *Apus apus? Journal of Avian Biology, 41*(1), 94–98. https://doi.org/10.1111/j.1600-048X.2009.04850.x.

Henningsson, P., Karlsson, H., Bäckman, J., Alerstam, T., & Hedenström, A. (2009). Flight speeds of swifts (*Apus apus*): Seasonal differences smaller than expected. *Proceedings of the Royal Society B: Biological Sciences, 276*(1666), 2395–2401. https://doi.org/10.1098/rspb.2009.0195.

Henningsson, P., Muijres, F. T., & Hedenström, A. (2011). Time-resolved vortex wake of a common swift flying over a range of flight speeds. *Journal of the Royal Society, Interface, 8*(59), 807–816. https://doi.org/10.1098/rsif.2010.0533.

Henningsson, P., Spedding, G. R., & Hedenström, A. (2008). Vortex wake and flight kinematics of a swift in cruising flight in a wind tunnel. *The Journal of Experimental Biology, 211*(5), 717–730. https://doi.org/10.1242/jeb.012146.

Horton, K. G., Doren, B. M. V., Stepanian, P. M., Farnsworth, A., & Kelly, J. F. (2016). Where in the air? Aerial habitat use of nocturnally migrating birds. *Biology Letters, 12*(11), 20160591. https://doi.org/10.1098/rsbl.2016.0591.

Jackson, B. E., Evangelista, D. J., Ray, D. D., & Hedrick, T. L. (2016). 3D for the people: Multi-camera motion capture in the field with consumer-grade cameras and open source software. *Biology Open, 5*(9), 1334–1342. https://doi.org/10.1242/bio.018713.

Karlsson, H., Henningsson, P., Bäckman, J., Hedenström, A., & Alerstam, T. (2010). Compensation for wind drift by migrating swifts. *Animal Behaviour, 80*(3), 399–404. https://doi.org/10.1016/j.anbehav.2010.05.023.

Kelly, J. F., Bridge, E. S., Frick, W. F., & Chilson, P. B. (2013). Ecological energetics of an abundant aerial insectivore, the purple martin. *PLoS One, 8*(9), e76616. https://doi.org/10.1371/journal.pone.0076616.

Knoppien, P., & Reddingius, J. (1985). Predators with two modes of searching: A mathematical model. *Journal of Theoretical Biology, 114*(2), 273–301. https://doi.org/10.1016/S0022-5193(85)80107-7.

Lack, D. (1956). *Swifts in a tower.* London, U.K: Meuthen.

Lack, D., & Lack, E. (1951). The breeding biology of the swift *Apus apus*. *Ibis, 93*(4), 501–546. https://doi.org/10.1111/j.1474-919X.1951.tb05457.x.

Le Bras, Y., Jouma'a, J., & Guinet, C. (2017). Three-dimensional space use during the bottom phase of southern elephant seal dives. *Movement Ecology, 5*, 18. https://doi.org/10.1186/s40462-017-0108-y.

Le Bras, Y., Jouma'a, J., Picard, B., & Guinet, C. (2016). How elephant seals (*Mirounga leonina*) adjust their fine scale horizontal movement and diving behaviour in relation to prey encounter rate. *PLoS One, 11*(12), e0167226. https://doi.org/10.1371/journal.pone.0167226.

Lentink, D., & de Kat, R. (2014). Gliding swifts attain laminar flow over rough wings. *PLoS One, 9*(6), e99901. https://doi.org/10.1371/journal.pone.0099901.

Lentink, D., Müller, U. K., Stamhuis, E. J., de Kat, R., van Gestel, W., Veldhuis, L. L. M., et al. (2007). How swifts control their glide performance with morphing wings. *Nature, 446*(7139), 1082–1085. https://doi.org/10.1038/nature05733.

Moore, T. Y., & Biewener, A. A. (2015). Outrun or outmaneuver: Predator-prey interactions as a model system for integrating biomechanical studies in a broader ecological and evolutionary context. *Integrative and Comparative Biology, 55*(6), 1188–1197. https://doi.org/10.1093/icb/icv074.

Mora, C. V., Ross, J. D., Gorsevski, P. V., Chowdhury, B., & Bingman, V. P. (2012). Evidence for discrete landmark use by pigeons during homing. *The Journal of Experimental Biology, 215*(19), 3379–3387. https://doi.org/10.1242/jeb.071225.

Rattenborg, N. C. (2017). Sleeping on the wing. *Interface Focus, 7*(1), 20160082. https://doi.org/10.1098/rsfs.2016.0082.

Reddy, G., Celani, A., Sejnowski, T. J., & Vergassola, M. (2016). Learning to soar in turbulent environments. *Proceedings of the National Academy of Sciences, 113*(33), E4877–E4884. https://doi.org/10.1073/pnas.1606075113.

Rothgänger, G., & Rothgänger, H. (1973). Über spezielle Verhaltensweisen fliegender Mauersegler. *Der Falke, 20*, 124–130.

Shelton, R. M., Jackson, B. E., & Hedrick, T. L. (2014). The mechanics and behavior of cliff swallows during tandem flights. *The Journal of Experimental Biology, 217*(15), 2717–2725. https://doi.org/10.1242/jeb.101329.

Shepard, E. L. C., Lambertucci, S. A., Vallmitjana, D., & Wilson, R. P. (2011). Energy beyond food: Foraging theory informs time spent in thermals by a large soaring bird. *PLoS One, 6*(11), e27375. https://doi.org/10.1371/journal.pone.0027375.

Shepard, E. L. C., Ross, A. N., & Portugal, S. J. (2016a). Moving in a moving medium: New perspectives on flight. *Philosophical Transactions of the Royal Society B: Biological Sciences, 371*(1704). https://doi.org/10.1098/rstb.2015.0382.

Shepard, E. L. C., Williamson, C., & Windsor, S. P. (2016b). Fine-scale flight strategies of gulls in urban airflows indicate risk and reward in city living. *Philosophical Transactions of the Royal Society B: Biological Sciences, 371*(1704). https://doi.org/10.1098/rstb.2015.0394.

Sicurella, B., Caffi, M., Caprioli, M., Rubolini, D., Saino, N., & Ambrosini, R. (2015). Weather conditions, brood size and hatching order affect Common Swift *Apus apus* nestlings' survival and growth. *Bird Study, 62*(1), 64–77. https://doi.org/10.1080/00063657.2014.989193.

Theriault, D. H., Fuller, N. W., Jackson, B. E., Bluhm, E., Evangelista, D., Wu, Z., et al. (2014). A protocol and calibration method for accurate multi-camera field videography. *The Journal of Experimental Biology, 217*(11), 1843–1848. https://doi.org/10.1242/jeb.100529.

Tobalske, B. W. (2007). Biomechanics of bird flight. *The Journal of Experimental Biology, 210*(18), 3135–3146. https://doi.org/10.1242/jeb.000273.

Tobalske, B. W. (2010). Hovering and intermittent flight in birds. *Bioinspiration & Biomimetics, 5*(4), 045004. https://doi.org/10.1088/1748-3182/5/4/045004.

Wainwright, C. E., Stepanian, P. M., Reynolds, D. R., & Reynolds, A. M. (2017). The movement of small insects in the convective boundary layer: Linking patterns to processes. *Scientific Reports, 7*(1), 5438. https://doi.org/10.1038/s41598-017-04503-0.

Warrick, D. R. (1998). The turning- and linear-maneuvering performance of birds: The cost of efficiency for coursing insectivores. *Canadian Journal of Zoology, 76*(6), 1063–1079. https://doi.org/10.1139/z98-044.

Warrick, D. R., Hedrick, T. L., Biewener, A. A., Crandell, K. E., & Tobalske, B. W. (2016). Foraging at the edge of the world: Low-altitude, high-speed manoeuvering in barn swallows. *Philosophical Transactions of the Royal Society B: Biological Sciences, 371*(1704). https://doi.org/10.1098/rstb.2015.0391.

Weller, T. J., Castle, K. T., Liechti, F., Hein, C. D., Schirmacher, M. R., & Cryan, P. M. (2016). First direct evidence of long-distance seasonal movements and hibernation in a migratory bat. *Scientific Reports, 6*, 34585. https://doi.org/10.1038/srep34585.

Appendix

RSV location reconstruction error

Accounting only for the quantization of 3D space performed by the digital stereo image (distance measure) and the digital rotary encoders (camera aiming angle measure), theory predicts a random 3D location error of 0.13, 0.52 and 2.09 m at 100, 200 and 400 m from our tracking device, respectively (for base length = 1 m, image width = 1920, equivalent focal length = 0.416 m and 13 bits encoders; see formulae in de Margerie et al., 2015).

True error was first assessed during calibration videos ($N = 15$ calibrations, seven calibration points per calibration). Random 3D location error was measured as the SD of the reconstructed location of each calibration point, over 30–50 repeated measures for each point. The observed SD was on average 1.69 times the theoretical value expected, approaching 0.2, 0.8 and 4 m at 100, 200 and 400 m, respectively (see profile on Fig. A2). As discussed in de Margerie et al. (2015), this supplementary random error comes from several sources, for example residual optical and structural distortion of the device. Two calibration videos with large random error (twice the theoretical one on average over the seven calibration points) were considered unreliable, and the corresponding bird-tracking videos were not analysed. Random error yields noise in the flight track, which we partly removed through track smoothing (see Fig. A3).

In addition to random error, for each calibration point we computed the systematic 3D location error as the distance between the mean reconstructed location and the true location (known from a LIDAR 3D map, see Methods section). Systematic error amounted to 0.46% of the calibration point distance on average (range 0.00–2.08%, see Fig. A4). Systematic error can result from small residuals of the distance calibration model (see de Margerie et al., 2015). As it affects neighbouring locations in a track equally (nonlinear scaling error), it has little effect on the track tortuosity. Systematic error can also result from not setting the device perfectly horizontal (it was levelled in the field with a bull's-eye spirit-level). By comparing the measured and true height of calibration points, we report an average inclination error of 0.11° (range 0.01–0.32°). As the common swift's minimal glide angle is about 4.6° (Henningsson & Hedenström, 2011), we considered the error was low enough to remain uncorrected in the present study.

Last, in between calibrations, minute deformation of the mirror camera assembly due to heat expansion results in some distance measure drift. For this reason, we did not allow direct sunlight on the device, and performed a new calibration every hour. Moreover, we checked for drift by re-recording each calibration point at the end of each bird-tracking video, and comparing again the mean reconstructed distance to the true distance. The drift amounted to a 0.79% distance error on average (range 0.00–4.65%, see Fig. A5). Because scaling error, even nonlinear, has little effect on track tortuosity, this was considered acceptable for the present study, but calls for further structural improvement of the device. One tracking video that showed a drift >5% for one of the calibration points was considered unreliable and removed from the data set.

Interpolating passage times through the sphere surface

Call (x_c, y_c, z_c) the spatial coordinates of the centre *C*, where the animal is currently located, of a virtual sphere with radius ρ, and (x_{in}, y_{in}, z_{in}, t_{in}) and (x_{out}, y_{out}, z_{out}, t_{out}) the spatiotemporal coordinates of the inside and outside locations *I* and *O*, recorded just before and after the animal leaves the sphere. The vector $\overrightarrow{IO}$ intercepts the sphere surface at a location *P*. The passage time through the sphere's surface, corresponding to an exit ($t_{\mathrm{in}} < t_{\mathrm{out}}$) or entering ($t_{\mathrm{in}} > t_{\mathrm{out}}$) time, can therefore be interpolated as:

$$t_P = t_{\mathrm{in}} + (t_{\mathrm{out}} - t_{\mathrm{in}})IP/IO$$

where *IO* is the norm of the vector $\overrightarrow{IO}$ ($IO = [{d_x}^2 + {d_y}^2 + {d_z}^2]^{0.5}$, with $d_x = x_{\mathrm{out}} - x_{\mathrm{in}}$, $d_y = y_{\mathrm{out}} - y_{\mathrm{in}}$ and $d_z = z_{\mathrm{out}} - z_{\mathrm{in}}$), and *IP* is the norm of vector $\overrightarrow{IP}$. This distance can be easily determined by considering the plane on which the three locations (*I*, *O* and *C*) lie. For this purpose, *C* can be expressed in a new frame of reference based on a translation of the origin at *I* and three successive rotations. The first, Ω, performed around the *Z* axis, corresponds to the orientation of the vector $\overrightarrow{IO}$ in the *XY* plane ($\cos(\Omega) = d_x/d_{xy}$ and $\sin(\Omega) = d_y/d_{xy}$, with $d_{xy} = ({d_x}^2 + {d_y}^2)^{0.5}$), so as to express *C* in a frame of reference (*U*, *V*, *W*), whose first axis (*U*) is defined by the $\overrightarrow{IO}$ projection on the *XY* plane ($u_{\mathrm{in}} = v_{\mathrm{in}} = w_{\mathrm{in}} = 0$; $u_{\mathrm{out}} = d_{xy}$, $v_{\mathrm{out}} = 0$, $w_{\mathrm{out}} = d_z$):

$$u_c = (x_c - x_{\mathrm{in}})\cos(\Omega) + (y_c - y_{\mathrm{in}})\sin(\Omega)$$

$$v_c = (y_c - y_{\mathrm{in}})\cos(\Omega) - (x_c - x_{\mathrm{in}})\sin(\Omega)$$

$$w_c = z_c - z_{in}$$

For 2D movements restricted to the plane *XY* ($z_c = z_{\mathrm{in}} = z_{\mathrm{out}} = 0$), and therefore involving a virtual circle rather than a virtual sphere, simply by applying Pythagoras' theorem, one gets $\rho^2 = (IP - u_c)^2 + {v_c}^2$, with $IP > u_c$, and therefore $IP = u_c + (\rho^2 - {v_c}^2)^{0.5}$. For 3D movements, two additional rotations are required. The second rotation, Φ, performed around the *V* axis, corresponds to the orientation of $\overrightarrow{IO}$ orthogonally to the *XY* plane ($\cos(\Phi) = d_{xy}/IO$ and $\sin(\Phi) = d_z/IO$), so as to express *C* in a frame of reference (*U*′, *V*′, *W*′) whose first axis (*U*′) is defined by $\overrightarrow{IO}$ ($u'_{\mathrm{in}} = v'_{\mathrm{in}} = w'_{\mathrm{in}} = 0$; $u'_{\mathrm{out}} = IO$, $v'_{\mathrm{out}} = w'_{\mathrm{out}} = 0$):

$$u'_c = u_c \cos(\Phi) + w_c \sin(\Phi)$$

$$v'_c = v_c$$

$$w'_c = w_c \cos(\Phi) - u_c \sin(\Phi)$$

A third rotation by atan$_2$ (w'_c, v'_c) around the *U*′ axis makes it possible to express *C* in a final frame of reference (*U*″, *V*″, *W*″), whose first two axes (*U*″, *V*″) constitute a frame of reference for the plane in which the three locations lie:

$$u''_c = u'_c$$

$$v''_c = \left({v'_c}^2 + {w'_c}^2\right)^{0.5}$$

$$w''_c = 0$$

Then, the passage through the surface of the sphere corresponds to the passage through the circumference of a circle in the *U*″*V*″ plane. Therefore, *IP* can be computed as:

$$IP = u''_c + \left(\rho^2 - {v''_c}^2\right)^{0.5} = u'_c + \left(\rho^2 - {v'_c}^2 - {w'_c}^2\right)^{0.5}$$

$$\text{with} \begin{pmatrix} u'_c \\ v'_c \\ w'_c \end{pmatrix} = \begin{pmatrix} d_{xy}/IO & 0 & d_z/IO \\ 0 & 1 & 0 \\ -d_z/IO & 0 & d_{xy}/IO \end{pmatrix} \times \begin{pmatrix} d_x/d_{xy} & d_y/d_{xy} & 0 \\ -d_y/d_{xy} & d_x/d_{xy} & 0 \\ 0 & 0 & 1 \end{pmatrix} \begin{pmatrix} x_c - x_{\mathrm{in}} \\ y_c - y_{\mathrm{in}} \\ z_c - z_{\mathrm{in}} \end{pmatrix}$$

Table A1

Correlation coefficients and statistics for original and modified data sets

	Mean	SD	*t*	*df*
Full data set, ρ = 30 m				
RT vs RL	0.97	0.04	189.16	56
RT vs *V*	−0.55	0.30	−13.77	56
RT vs *F*	0.27	0.33	5.69	49
RT vs *Vz*	0.25	0.28	6.78	56
Full data set, ρ = 20 m				
RT vs RL	0.95	0.06	111.01	56
RT vs *V*	−0.56	0.27	−15.87	56
RT vs *F*	0.23	0.26	6.15	49
RT vs *Vz*	0.23	0.23	7.70	56
Full data set, ρ = 40 m				
RT vs RL	0.98	0.03	222.70	56
RT vs *V*	−0.55	0.35	−11.95	56
RT vs *F*	0.31	0.38	5.70	49
RT vs *Vz*	0.26	0.35	5.63	56
Data set after removing locations involving social interactions, ρ = 30 m				
RT vs RL	0.97	0.04	191.42	56
RT vs *V*	−0.54	0.31	−13.12	56
RT vs *F*	0.24	0.33	5.23	49
RT vs *Vz*	0.23	0.30	5.92	56

All *P* values are less than 0.0001.

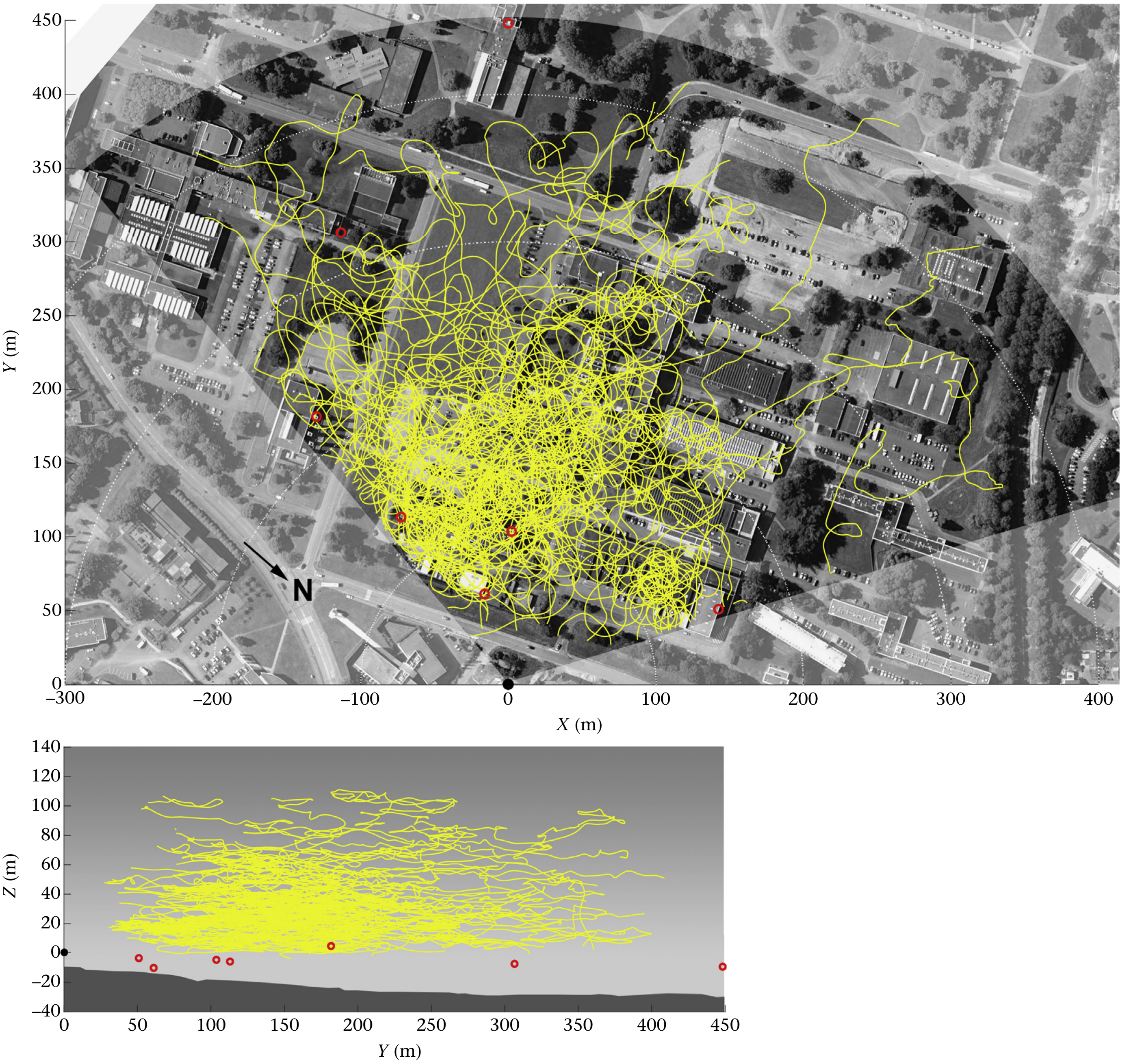

Figure A1. Overview of swift flight tracks. (a) *X/Y* projection showing all 57 flight tracks (yellow) superimposed on aerial photography of the study site in Rennes, France (48.121N, 1.634W). The black dot at [0, 0] coordinates represents the RSV device. Red circles show the seven points used for distance calibration (salient objects on buildings' roofs). The lighter area delimits the 'study area' (ca. 2.2×10^5 m^2, corresponding to a sampling volume of ca. 5.8×10^7 m^3). (b) Side view (*Y/Z* projection) with ground level represented in darker grey. Source for aerial photography and ground level: Institut Géographique National.

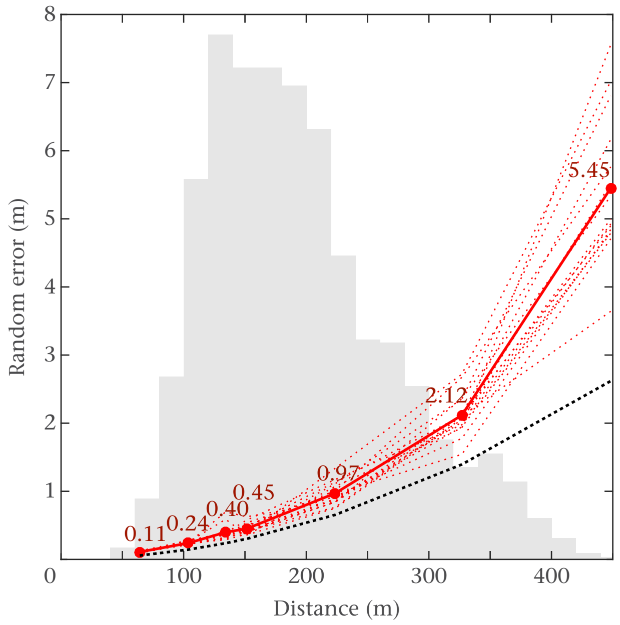

Figure A2. Random error in 3D location reconstruction, as a function of distance from the RSV device. Red dots: mean error for calibration points. Red dotted lines: error for individual calibrations. Black dotted line: theoretical random error from 3D space quantization only. The background histogram shows the distance distribution for all sampled bird locations.

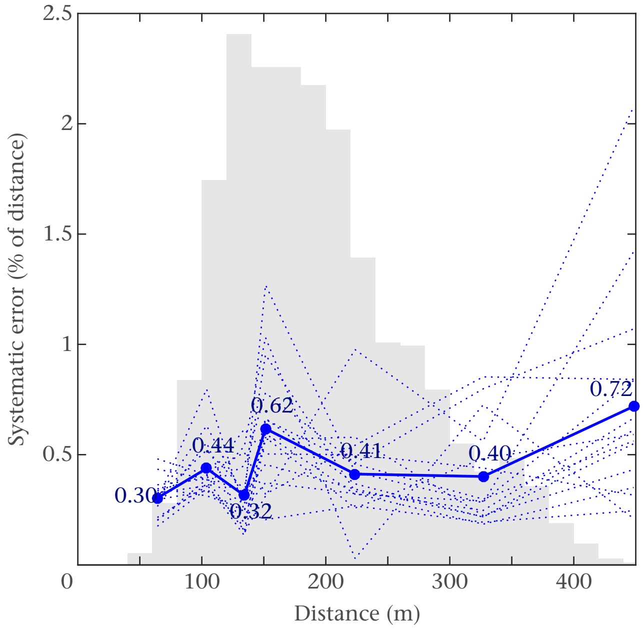

Figure A4. Systematic error in 3D location reconstruction, as a function of distance from the RSV device. Blue dots: mean error for calibration points. Blue dotted lines: error for individual calibrations. The background histogram shows the distance distribution for all sampled bird locations.

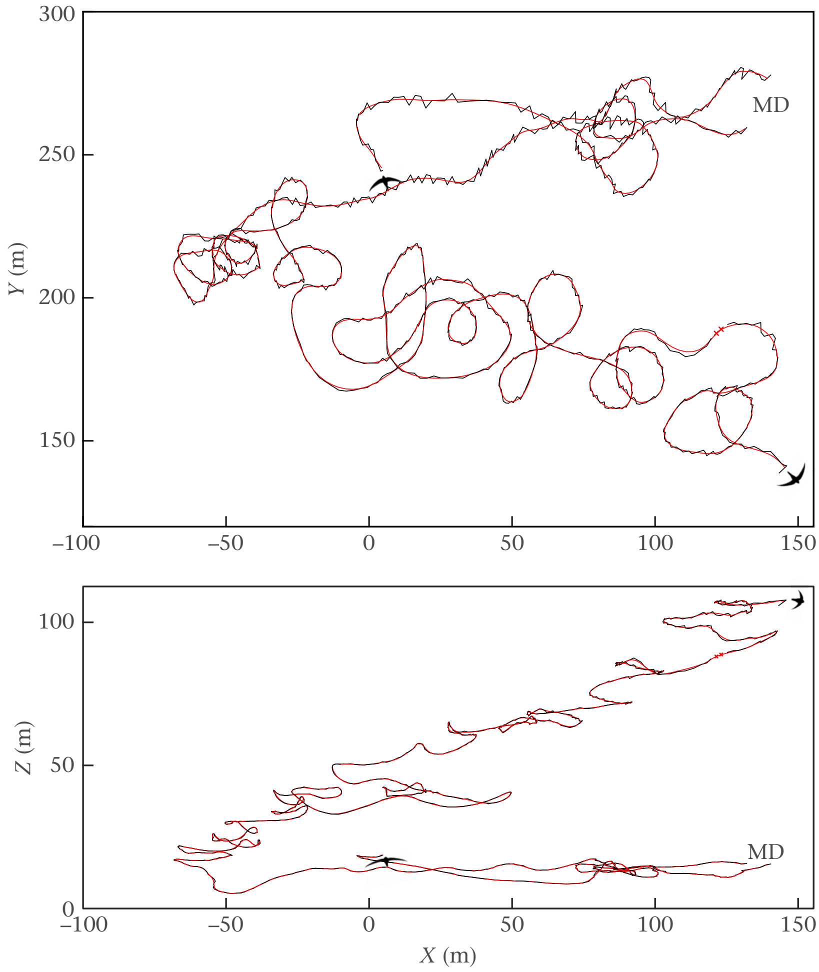

Figure A3. Example of track random error filtering, using spline smoothing (Garcia, 2010). Ground-based track, relative to RSV device situated at coordinates [0, 0, 0], is shown in top (*X*/*Y*) and side (*X*/*Z*) views. The raw track from RSV is traced in black, the smoothed track in red. Red crosses indicate two missing locations that were interpolated. A longer missing segment (MD) of 14 locations was too long (>9 locations) to be reliably interpolated, thus remained as missing data. The distance-dependent noise amount in the raw track is apparent in the top view, when comparing closer (minimal distance to RSV device 170 m) with more distant track segments (maximal distance 310 m). The bird drawings indicate flight direction and are not to scale (ca. ×30).

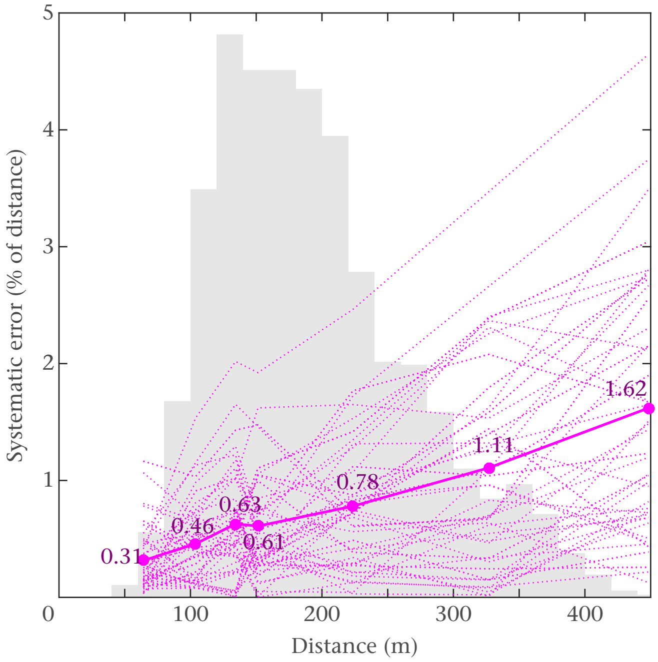

Figure A5. Effect of calibration drift on systematic error in location distance reconstruction, as a function of distance from the RSV device. Purple dots: mean error for calibration points refilmed during bird-tracking videos. Purple dotted lines: error for individual bird-tracking videos. The background histogram shows the distance distribution for all sampled bird locations.

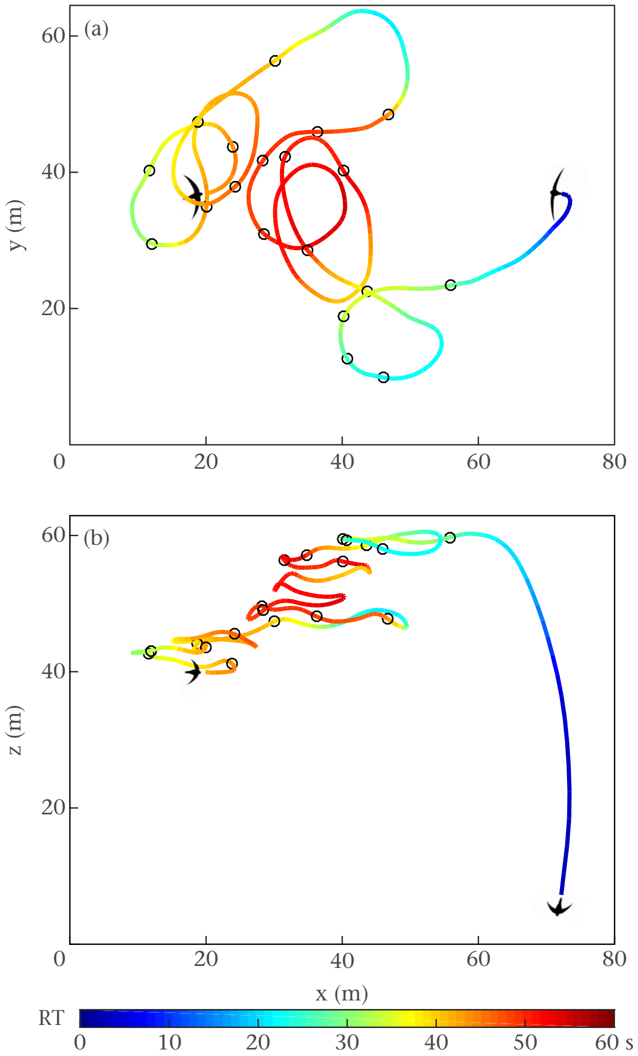

Figure A6. Example of a common swift performing a steep dive after a period of VCS in a thermal updraft. (a) Top view; (b) side view. Black circles indicate atypical flight postures. Track duration is 60 s, track length is 428 m. RT: residence time. The bird drawings indicate flight direction and are not to scale (ca. ×15).